Journal of Hazardous Materials 192 (2011) 490–499

Contents lists available at ScienceDirect

Journal of Hazardous Materials

journal homepage: www.elsevier.com/locate/jhazmat

Relating organic fouling of reverse osmosis membranes to adsorption during the reclamation of secondary effluents containing methylene blue and rhodamine B

Haigang Li[a], Yanwen Lin[a], Yunbai Luo[a], Ping Yu[a,*], Liwei Hou[b]

[a] College of Chemistry and Molecular Science, Wuhan University, Wuhan 430072, PR China
[b] School of Resource and Environmental Science, Wuhan University, Wuhan 430079, PR China

ARTICLE INFO

Article history:
Received 20 January 2011
Received in revised form 8 May 2011
Accepted 15 May 2011
Available online 20 May 2011

Keywords:
Dyes fouling
Irreversible sorption
Fouling kinetics
Irreversible flux decline

ABSTRACT

Dyes fouling of reverse osmosis (RO) membranes and its relation to adsorption had been investigated by using a crossflow RO filtration setup. Methylene blue (MB) and rhodamine B (RB) were used as model organic foulants. The calculated amount of the irreversible sorption was related to the irreversible flux decline. The characteristic fouling kinetics was accounted by Langmuir–Hinshelwood (L–H) kinetics model for initial fouling, with the fouling rate constant $k = 0.0556\ \mu m\ s^{-1}\ min^{-1}$ and $k = 0.0181\ \mu m\ s^{-1}\ min^{-1}$ for MB and RB fouling RO membrane CPA2, respectively. And the subsequent fouling was attributed to the growth of a dye cake. A remarkable correlation was obtained between the quantified irreversible sorption and irreversible flux decline under the solution chemistries investigated. In the presence of divalent cation, the extent of flux decline was related to the competition model.

1. Introduction

The reclamation of industrial wastewater is paramount important for keeping up with the soaring water demand in the world. Among water recycling technologies, reverse osmosis (RO) is one promising option because of the efficiency in the simultaneous removal of hydrated salt ions and larger solutes from process water or wastewater, irrespective of their charge [1]. Nevertheless, organic fouling of RO membranes has been a recalcitrant obstacle to an efficient application in RO technology [2,3]. Membrane fouling results in the decline in water quantity and quality. In the case of pretreated secondary wastewater in the textile industry, dyes are the primary constituents [4]. The presence of dyes causes RO flux decline in the membrane-based purification of wastewater for recycling.

Several fouling mechanisms have been described in the literature [5–7]. Fouling can occur in two ways: fouling layer formation and adsorption of foulants [8]. Cake fouling can be sensibly decreased after water backwashing or back-flushing. While, fouling due to the adsorption of foulants can only be counteracted to a certain extent by aggressive chemical cleaning. Furthermore, fouling can be affected by the interaction between foulants. When the feed contains a mixture of contaminants, the adsorption of a single foulant decreases by competitive sorption processes [9]. But the fouling is more severe due to the synergistic effect [10]. Meanwhile, the surfactants fouling will decrease when the concentration is higher than critical micelle concentration (CMC) due to the micellisation [5]. Initial fouling is controlled by the interaction between the bulk foulants and the membrane surface, while intermolecular adhesion between the bulk foulants and the foulants adsorbed on the membrane surface primarily controls the evolution of the fouling layer [2]. Hence, the flux decline in aqueous solutions containing organic compounds is mainly caused by adsorption [6,11], enhanced by cake formed on the membrane surface.

The influence of free calcium on organic fouling has been studied by several researchers [12,13]. Its presence was observed to aggravate fouling phenomenon as bridging agents with organic compounds, forming highly compacted gels [14]. In addition, this complexation has been explained by the egg-box model [2,15]. Particularly interesting is the finding that the opposite effect was also observed with fatty acids owing to the decreasing organic hydrophobicity after calcium addition [3,16]. The effect of magnesium on organic fouling, previously uncharted [17], has become an emerging field recently [14,18,19]. Membrane fouling increases slightly in the presence of magnesium compared to calcium. The anomaly in the fouling profile is attributed to salting-out effect on protein fouling [18]. S. Lee et al. [19] have confirmed that a thick alginate gel layer was visible when the

* Corresponding author. Tel.: +86 27 68772263; fax: +86 27 68776726.
E-mail address: yuping@whu.edu.cn (P. Yu).

0304-3894/$ – see front matter © 2011 Elsevier B.V. All rights reserved.
doi:10.1016/j.jhazmat.2011.05.044

Nomenclature

q	adsorption capacity (μmol/m^2)
C	concentration (μM)
t	permeation measuring time (min)
J	permeation flux (ml/(m^2 min))
V	volume (L)
A	the effect membrane area (m^2)
S	adsorption amount (μmol)
R	rejection
a	the rate constant for the exponential decline in $C_{feed}(t)$ (min^{-1})
b	the rate constant for the exponential decline in $R(t)$ (min^{-1})
r	initial fouling rate (μm s^{-1} min^{-1})
k	fouling rate constant (μm s^{-1} min^{-1})
K	Langmuir adsorption coefficient (s μm^{-1})
FR	flux recovery

Greek letters

θ	contact angle (°)

Subscript/superscript

final	the end of fouling
0	initial state
Feed	feed solution
SS	steady state
ir	irreversible
re	reversible
c	chemical cleaning solution
wc	cleaned membrane
ww	fouled membrane
wi	virgin membrane
pe	permeate flux

fouling was performed in the presence of calcium, but invisible in the presence of magnesium. The membrane surface property also plays an important role on the membrane fouling. The permeate flux tends to be more decreasing as membrane surface becomes rougher, more hydrophobic and neutral or negative charge [20].

Although many models were used to describe the fouling, there is currently no model discriminate the initial fouling and the subsequent fouling. The motivation for this study was to discriminate the fouling occurred in the initial stage and long time. Organic fouling was elucidated during the initial stages by Langmuir–Hinshelwood (L–H) kinetics model and then by cake filtration. MB and RB were selected as model contaminants because of their being widely used as colorants in textiles. The calculated amount of the irreversible sorption was related to the irreversible flux decline. The influences of the initial flux, the initial concentration and divalent cations were systematically studied.

2. Materials and methods

2.1. RO membranes

Characteristics of the three types of RO membranes are summarized in Table 1. According to the application data given by supplier, the maximum feed solution turbidity is 1.0 NTU for all RO membranes. The membranes coupons were stored in deionized (DI) water at 4 °C with water replaced regularly prior to experiments.

Membrane surface roughness was determined by atomic force microscopy (AFM) analysis (SPM-9500J3, SHIMADZU, Kyoto, Japan), quantified by root mean square (RMS) roughness. RMS is the deviation of the peaks and valleys from the mean plane [21].

Contact angle measurements were performed with an automated contact angle goniometer (DSA100; KRŰSS GmbH, Hamburg, Germany). At least 12 contact angle measurements were performed and the highest and lowest values were discarded before taking the average.

Zeta-potential of the membranes surface was determined by a streaming current electro kinetic analyzer (SurPass, Anton Paae GmbH, Graz, Austria). The zeta-potential was calculated based on Fairbrother-Mastin approach [22], and 10 mM KCl was used as background electrolyte solution.

The attenuated total reflection-Fourier transform infrared (ATR-FTIR) spectroscopy analyses were performed by using the Nicolet AVATAR 360 FT-IR Spectrophotometer. ATR-FTIR spectra measurements were performed at 10 different locations, with each spectrum averaged from 64 scans.

In addition, the surface of the membrane was analyzed by using a scanning electron microscopy (SEM) (FEI Quanta 200, Holland).

2.2. Organic foulants and reagents

MB and RB were purchased from Sinopharm Chemical Reagent Co., Ltd. (Shanghai, China). For preparation of solutions, a stock solution with concentration of 1.0 mM was prepared. The ionic strength of the solutions was adjusted to the required concentration by NaCl stock solution (1 M), and the pH was adjusted by 0.1 M NaOH and 1.0 M HCl. Calcium chloride dehydrate ($CaCl_2{\cdot}2H_2O$) or magnesium chloride hexahydrate ($MgCl_2{\cdot}6H_2O$) (0.1 M) were used to adjust the bivalent cation concentration of the bulk solution, while the total ionic strength was maintained constant by adjusting NaCl concentration. NaOH (pH 11), disodium ethylenediaminetetraacetate (Na_2-EDTA) (0.5 mM), NaCl solution (0.1 mM) and sodium dodecyl sulfate (SDS) (2 mM, pH 11) were used as cleaning agents because they are the most common compounds in commercial cleaning products for organic-fouled membranes [23]. The solution was freshly prepared with DI water before each experiment. The MB, RB, NaCl, $CaCl_2{\cdot}2H_2O$, $MgCl_2{\cdot}6H_2O$ and NaOH were analytical reagents. The EDTA and SDS were chemical reagents. The structure/size of the dyes molecules was analyzed by a nanoparticle size analyzer (ZEN 3600, Malvern Instrument, Malvern, UK). The turbidity of all the feed solutions is below 1.0 NTU, and the largest turbidity (6 μM MB solution) is 0.7 NTU.

Table 1
Characteristics of RO membranes used in this study.

Membrane type	RMS roughness (nm)	Zeta potential[a] (mV)	Contact angle (θ)	NaCl rejection (%)
PROC10	86.43	−11.25	26.41 ± 1.14	99.7[b]
CPA2	111.8	−20.13	22.38 ± 1.75	99.7[c]
ESPA2	80.22	−18.20	34.09 ± 0.88	99.6[c]

[a] Zeta potential is determined at pH 7.0.
[b] NaCl rejection is based on the standard test condition of 15.5 bar, 2000 mg/L and 25 °C.
[c] NaCl rejection is based on the standard test condition of 15.5 bar, 1500 mg/L and 25 °C.

2.3. Lab-scale crossflow experiments

In the experimental trials, a laboratory-scale crossflow test unit was employed. The crossflow test unit consists of a round membrane cell, high-pressure pump, electromagnetic mixer, feed reservoir and temperature control system. The test solution was held in a 3.0 L reservoir and fed to the membrane cell by the high-pump (Jingqiao, JW-C, Jingxin Pump Manufacturing Co., Ltd., Huai'an, China). The effect surface area of the membrane in contact with feed solution was 46.5 cm^2. The system was operated in a closed-loop mode and both permeate and retentate were recirculated into the feed reservoir.

When investigating the influence of feed chemistry on fouling, the initial flux and the crossflow velocity were fixed at <!– no-mfc –>2.1×10^{-5} m/s<!– /no-mfc –> and <!– no-mfc –>9.8×10^{-2} m/s<!– /no-mfc –>, respectively. Similarly, the feed solution chemistry was fixed when investigating the influence of the initial flux on fouling. Feed flow rate and desired pressure were achieved by adjusting the bypass valve and back-pressure regulator. The initial flux is conducted from 16.5 to 29.5 $\mu m\, s^{-1}$, and the relevant transmembrane pressure is 1.5, 1.7, 2.0, 2.5, 3.0 and 3.5 Mpa.

The membrane was first compacted with DI water (foulant-free) at 20.7 bar (300 psi) for at least 12 h. Then the membrane was stabilized and equilibrated for 6.0 h with the foulant-free electrolyte solution having solution chemistry identical to that used for the subsequent fouling stage. After attaining a stable permeate flux, the initial flux and the crossflow velocity were adjusted to the desired value. Fouling was initiated by adding the dissolved foulants stock solution to the feed tank to achieve the desired foulant concentration. The permeate flux was continuously monitored for the next 12 h.

At the end of the fouling experiments, the fouled membrane was cleaned by the chemical cleaning solution for 1 h. The solution was continuously circulated from the feed tank to the membrane in the cell at the normal atmosphere. At the end of cleaning, the chemical cleaning solution in the reservoir was disposed off and the reservoir and the membrane cell were rinsed with DI water to flush out the residual solution. Finally, the foulant-free electrolyte solution flux after chemical cleaning was measured to determine the extent of irreversible flux decline.

2.4. Adsorption test

Adsorption experiments for the samples were undertaken in the laboratory-scale crossflow test unit. The solution was continuously circulated from the feed tank to the membrane in the cell at the desired pressure and 30 °C. Permeate flow was recycled to the feed tank, too. Samples of 1.5 mL were taken by syringe at different time intervals. Concentration of dyes was determined with a UV-visible spectrophotometer (UV-1700, SHIMADZU, Kyoto, Japan) by measuring absorbance at 664 and 551 nm for λ_{max} of MB and RB, respectively [24,25]. The amount of solute adsorbed on the membrane, q_t ($\mu mol/m^2$), was calculated using Eq. (1) at the initial fouling stage.

$$q_t = \frac{(C_0 - C_t)V}{A} \tag{1}$$

where C_0 and C_t are concentrations of the dyes in solution (μM) at time $t = 0$ and $t = t$, respectively. V is the volume of the solution (L) and A is the effective membrane area (m^2).

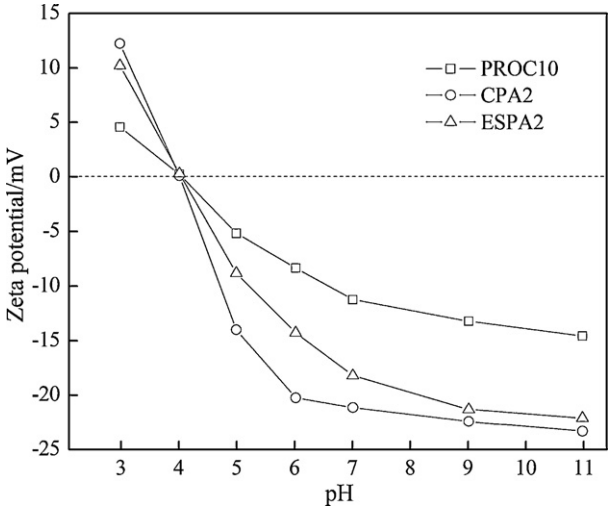

Fig. 1. Changes of zeta potential of RO membranes against solution pH.

At the end of fouling, the feed concentration declined significantly, so it is necessary to use the more complex form of the equation for the total amount sorbed, following Eq. (2) [26].

$$S_{final} = JC^{ss}_{feed}\frac{R_o - R_{ss}}{b} + J\frac{(C^{ss}_{feed} - C^{0}_{feed})(R_o - R_{ss})}{a+b} \tag{2}$$

where S_{final} is the total amount of solute adsorbed on the membrane at the end of fouling (μmol), J is the permeate flux at the end of fouling (L/min), C^{ss}_{feed} is the steady-state feed concentration (μM), C^{0}_{feed} is the initial feed concentration (μM), R_0 is the initial rejection of the solute, R_{ss} is the steady-state rejection of the solute, a is the rate constant for the exponential decline in $C_{feed}(t)$ (h^{-1}), b is the rate constant for the exponential decline in $R(t)$ (h^{-1}).

So, the amount of solute adsorbed on the membrane, q_{final} ($\mu mol/m^2$), was calculated using Eq. (3) at the end of fouling.

$$q_{final} = \frac{S_{final}}{A} \tag{3}$$

At the end of cleaning, the reversible and irreversible adsorption is determined by Eq. (4) and Eq. (5), respectively.

$$q_{re} = \frac{\sum C_c V_c}{A} \tag{4}$$

$$q_{irr} = q_{final} - q_{re} \tag{5}$$

where q_{re} and q_{irr} are the reversible and irreversible adsorption, respectively. C_c is the dye concentration in the chemical cleaning solution (μM) and V_c is the volume of the cleaning solution (L).

3. Results and discussion

3.1. Characterization of RO membranes

Fig. 1 plotted changes of zeta-potential for three different types of RO membranes with respect to solution pH. The amphoteric behavior with isoelectric points around pH 4.0 is ascribed to both amine and carboxylic functional groups existing in aromatic polyamide chains in membrane surface [27]. The observation that PROC10 has the least negative zeta-potential (−11.25 mV) at neutral pH suggests that the polyamide layer is more intense.

ATR-FTIR spectra of virgin RO membranes were obtained to verify functional groups of the membrane. The typical ATR-FTIR

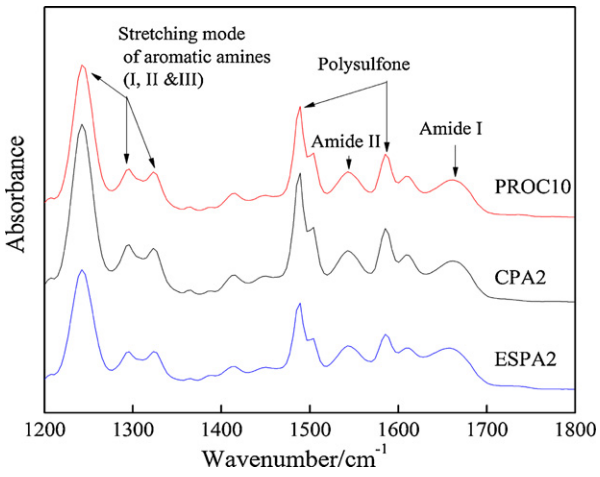

Fig. 2. ATR-FTIR spectra of the virgin RO membranes.

spectra are shown in Fig. 2. The spectra of virgin membranes show the main characteristic bands: 1243, 1295 and 1327 cm^{-1} assigned to aromatic amines I, II and III stretching [27,28], 1490 and 1585 cm^{-1} assigned to polysulfonyl group in the polysulfone layer, 1545 cm^{-1} assigned to amides I and 1665 cm^{-1} assigned to amides II. Amines and polysulfonyl groups of RO membranes are confirmed and all the spectra look similar.

AFM images of the virgin membranes are presented in Fig. 3. The AFM images clearly show that all membranes exhibit large scale surface roughness of ridge-and-valley structure and the membrane CPA2 exhibits the largest scale. The distinctly rough morphology is an inherent property of interfacially polymerized aromatic polyamide composite membranes [17]. And the surface morphology could influence on the initial membrane fouling [17,27].

3.2. Fouling mechanism

3.2.1. Initial stages of organic fouling

Reduction of available site for membrane filtration leads to permeate flux decline. Surface fouling is the dominant fouling mechanism for RO and involves the initial stages of fouling and the subsequent growth of a fouling layer [2]. The L–H kinetics rate model was applied to the surface fouling of organic compounds. This situation is in contrast to the research on the heterogeneous degradation of many organic contaminations [29–31]. The rate law is given by

$$r = \frac{-kKJ}{1+KJ} \tag{6}$$

where r is the initial rate of flux decline ($\mu m\, s^{-1}\, min^{-1}$) and $r = -dJ/dt$, k is the fouling rate constant ($\mu m\, s^{-1}\, min^{-1}$), K is the Langmuir adsorption coefficient ($s\, \mu m^{-1}$), J is the membrane flux at time t ($\mu m\, s^{-1}$).

Eq. (6) is then integrated analytically to the algebraic solution and can be rewritten in Eq. (7).

$$\frac{\ln(J_0/J)}{J_0 - J} = kK\frac{t}{J_0 - J} - K \tag{7}$$

where J_0 is the initial permeate flux of membranes ($\mu m\, s^{-1}$).

Laboratory flux data for the first 1 h transformed using the L–H kinetics rate model are shown in Fig. 4. In all cases, the initial portion of the curve increased in a straight line fashion with a related coefficient very near 1.0 demonstrating that the initial stages of flux decline induced by organic adsorption quantitatively corresponded to the L–H kinetics rate model.

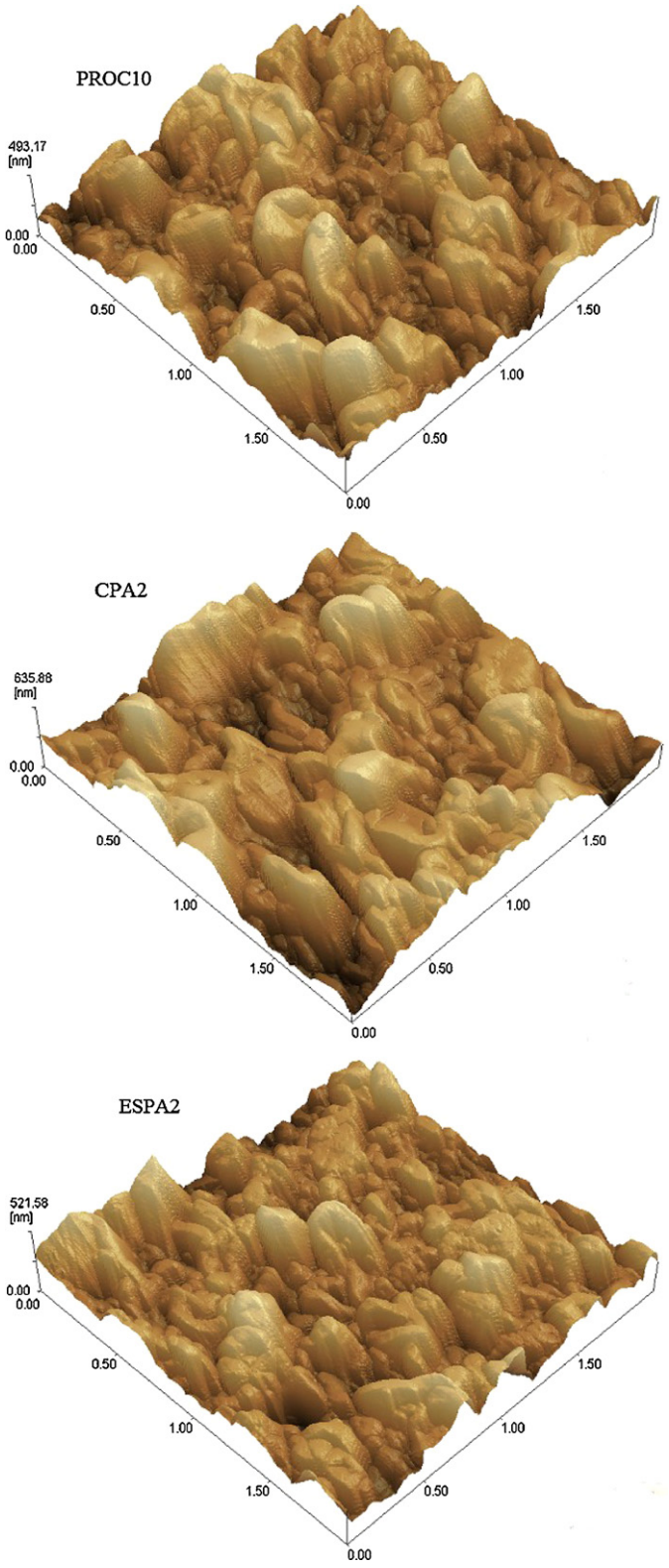

Fig. 3. AFM images of the virgin RO membranes. Each side of plane is 2 μm with the height of 521.58 nm.

A linear regression fit between the flux decline and the adsorbed mass on the membrane surface is shown in the inset of Fig. 4. A striking correlation is displayed for the runs with MB and RB. This

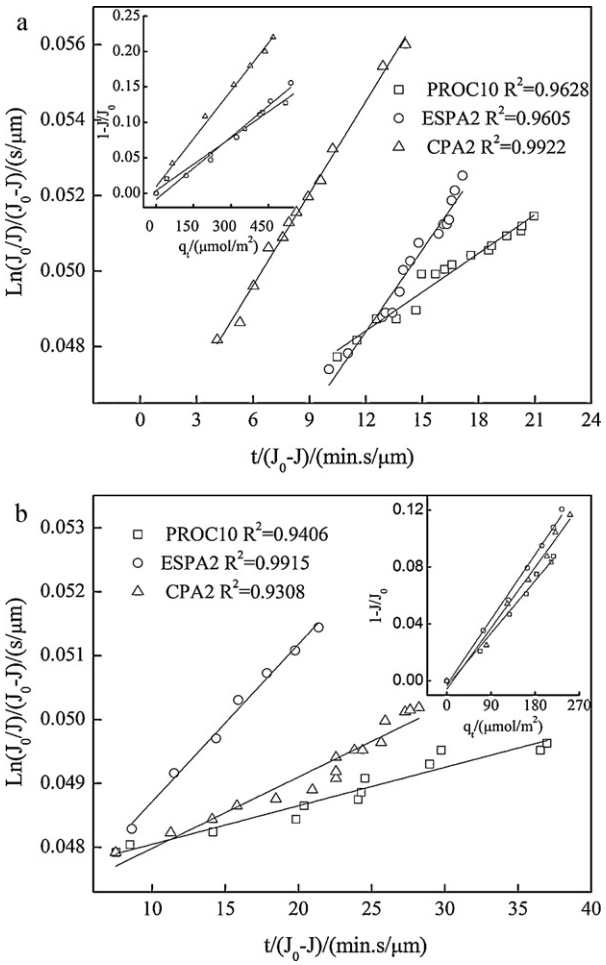

Fig. 4. Linear regression fit of the Langmuir–Hinshelwood equation at the initial stage for (a) MB fouling and (b) RB fouling. The insets show correlation between the flux decline and the adsorption mass on the membrane surface. Experimental conditions: dye concentration = 2.0 μM, ionic strength = 10 mM, pH = 7.0 and temperature = 30 ± 0.5 °C.

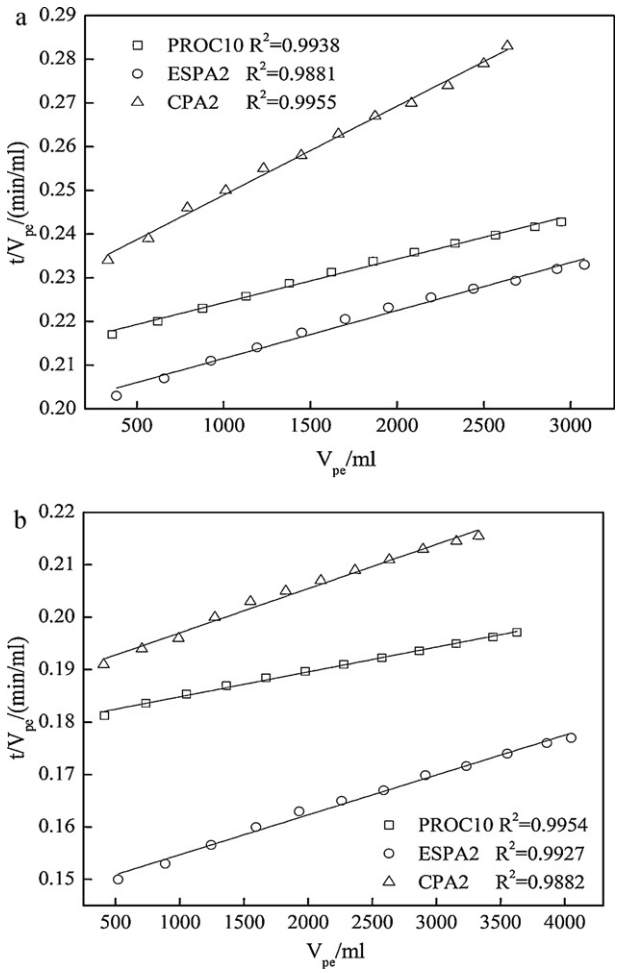

Fig. 5. The classical cake filtration model at the long time for (a) MB fouling and (b) RB fouling. Experimental conditions were identical to those in Fig. 4.

direct relationship between the flux decline and the adsorbed mass confirms that adsorption plays a key role in the flux decline [6,11]. As can be seen from Fig. 4, the adsorption of MB is greater than that of RB. This is attributed to the carboxylic group in structure of RB. RB has zwitterionic character because of the dissociation of carboxylic group [24] at pH 7.0. As a result, the amount of the adsorption is low due to the electrostatic repulsion between RB and the membrane surface. And the better a component adsorbs on the membrane surface, the more flux decline is observed. As depicted in the inset of Fig. 4, the flux through the membrane CPA2 decreases at the fastest rate among the three membranes. This behavior is attributed to the highest initial flux because of the largest scale surface roughness at the fixed pressure.

3.2.2. Specific cake formation

A good agreement with the L–H model at short times has been obtained. However, at long times the data shows significant deviation from linearity due to the flux through the fouled membrane (not shown). The transition takes place within 1.0 h fouling. The classical cake filtration model predicts that a plot of time (t) divided by permeate volume (V_{pe}) should be linear in V_{pe} [32,33]. Fig. 5 ((a) MB fouling and (b) RB fouling) represents the profile of t/V_{pe} versus V_{pe} for the next 11 h. SEM micrographs of virgin and fouled membranes (Fig. 6) clearly confirm the formation of a cake layer on the membrane surface. All the images of virgin membranes show pebble-style surface with peak and valley structures attributed to the top facial polyamide layers [20].

The results from Figs. 4 and 5 clearly indicate that fouling is controlled first by the adsorption of organic compounds and then by cake formation.

3.3. Membrane cleaning with various chemical reagents

In this section, conditions for fouling experiments were dyes concentration 2.0 μM, pH 7.00 ± 0.05 and temperature 30.0 ± 0.05 °C. Fig. 7 describes the degree of recovery of the fouled membranes in terms of DI water containing salts (the same ionic strength as the fouling run) flux by chemical cleaning with various reagents. Flux recovery (FR) used for demonstrating the cleaning efficiency can be calculated [34] as Eq. (8):

$$\mathrm{FR}(\%) = \left[\frac{J_{wc} - J_{ww}}{J_{wi} - J_{ww}}\right] \times 100 \quad (8)$$

where J_{wc}, J_{ww} and J_{wi} are cleaned membrane permeate flux (μm s^{-1}), fouled membrane permeate flux (μm s^{-1}) and virgin membrane permeate flux (μm s^{-1}), respectively.

As described in Fig. 7, membranes fouled by RB were slight compared to by MB. This is attributed to the preferential adsorption of MB compared to RB on the membrane surface. For all membranes and both dyes, the cleaning efficiency follows the same order of decline: SDS (2 mM, pH 11.0) > NaOH (pH 11.0) > EDTA (0.5 mM) > NaCl (0.1 M) > DI water.

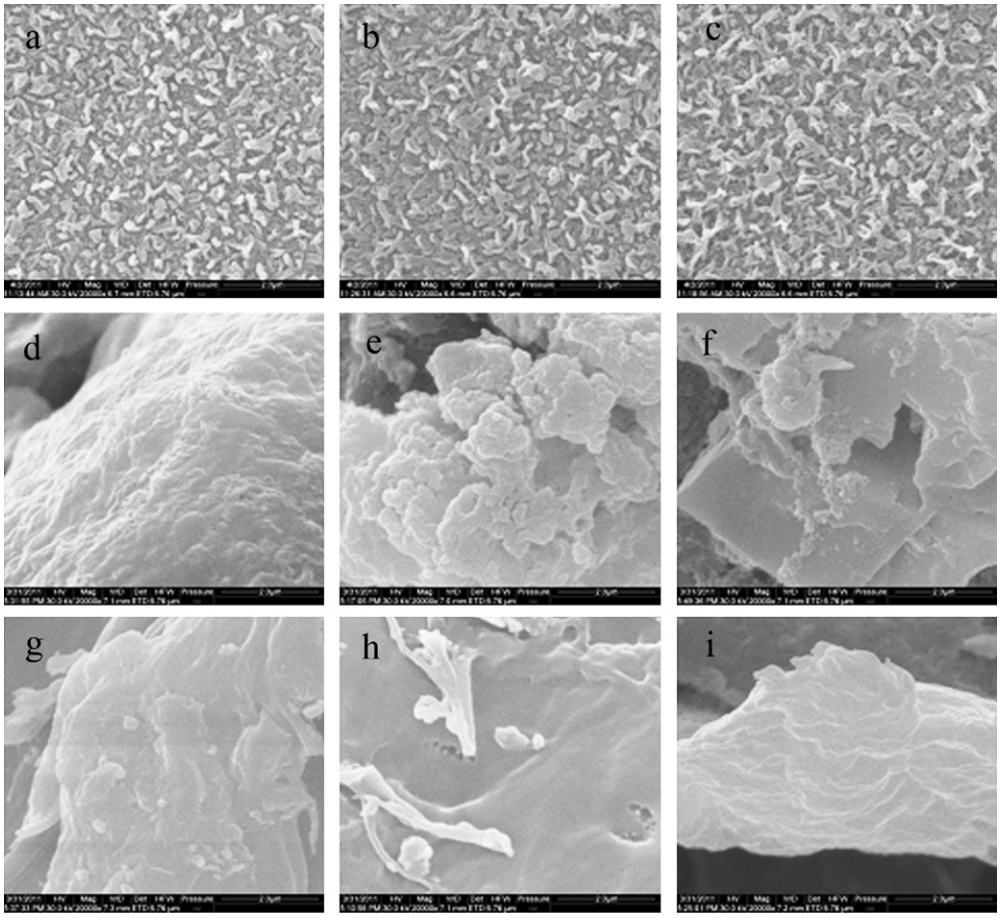

Fig. 6. SEM images of virgin and fouled membranes with 20,000 times magnification: (a) virgin PROC10, (b) virgin CPA2, (c) virgin ESPA2, (d) MB fouling PROC10, (e) MB fouling CPA2, (f) MB fouling ESPA2 fouled, (g) RB fouling PROC10, (h) RB fouling CPA2, (i) RB fouling ESPA2.

The cationic dyes are easily adsorbed onto the negatively charged membrane surface. In the case of NaOH cleaning, dye molecules and membrane surface are charged more negatively, resulting in desorption of dye molecules from the membrane surface. EDTA, as a metal chelating agent, removes foulants from membrane surface through a ligand-exchange reaction [23]. NaCl solution cleaning involves structural changes of the cross-linked gel layer on the membrane surface by an ion exchange reaction [35]. SDS molecules will decrease the surface tension of adjacent molecules. According to the results, SDS solution was selected as the effective agent to determine the extent of irreversible flux decline.

3.4. Flux-decline behaviors

3.4.1. Effects of the initial flux

The influence of initial flux on dyes fouling CPA2 membrane is presented in Fig. 8. All fouling experiments were performed at the same dye concentration (2 μM), solution chemistry (ionic strength 10 mM and pH 7.0), and crossflow velocity (<!– no-mfc –>9.8 cm/s<!– /no-mfc –>). The initial flux was controlled by adjusting the trans-membrane pressure for each fouling run. As shown in Fig. 8, the higher the initial flux, the greater the fouling rate, and the result is quite well accorded with previous studies [17,19,36]. The higher dye molecules transport rate results in greater rate of dye molecules deposition onto the membrane surface and, subsequently, increases rate of membrane fouling. In addition, the higher pressure also results in greater rate of dye molecules absorbed onto the membrane surface. Furthermore, at higher initial flux, the dye fouling layer becomes more compressed, leading to an increasing hydraulic resistance to permeate flow.

The L–H kinetics rate model was applied to the organic fouling. Fouling rate was determined from the slope of the linear region of the flux decline curve with respect to the filtration time. A non-linear regression fit of the L–H equation is shown in the inset of Fig. 8 indicating $k = 0.0556\ \mu m\ s^{-1}\ min^{-1}$ for MB fouling and $k = 0.0181\ \mu m\ s^{-1}\ min^{-1}$ for RB fouling. The calculated value of k for MB fouling is higher than it for RB fouling, thus again confirming our finding regarding MB fouling more severe compared to RB.

3.4.2. Effects of the initial concentration

Fig. 9 clearly illustrates the influence of the initial concentration on the flux decline during the fouling experiment at pH 7.0. As presented in Fig. 9, the initial fouling rate increased with the increasing dye concentration at fixed ionic strength. However, it is noted that further increase in dye concentration results in a negligible increase on the initial fouling rate, especially the fouling behavior observed with RB. The similar phenomenon was observed through the reversibility of flux loss. Another interesting finding was that the fouling tended to decrease at RB concentration 6 μM.

The membrane surface was negatively charged at pH 7.0. Therefore, cationic dyes can be adsorbed onto the membrane surface easily. The fouling was directly controlled by the amount of adsorption. It has been reported that adsorption of organic dyes on various adsorbents usually obeys Langmuir isotherm [24,37,38]. As shown in the inset of Fig. 9a, adsorption of MB on PROC10 membrane obeys Langmuir isotherm. The interaction between dyes and the membrane is mainly controlled by dyes concentration. Hence, the

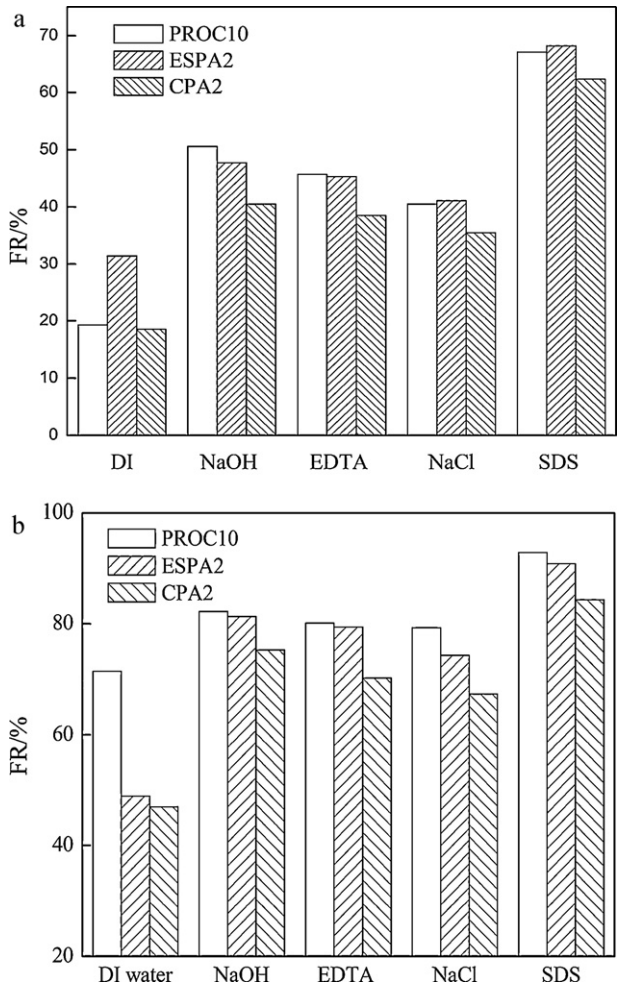

Fig. 7. Influence of cleaning solution type on cleaning of organic fouled RO membranes: (a) MB fouling and (b) RB fouling. Conditions for cleaning experiments: time = 1 h, temperature = 30.0 ± 0.05 °C, crossflow <!– no-mfc –>velocity = 30.5 cm/s<!– /no-mfc –>. Cleaning solutions were used at ambient pH.

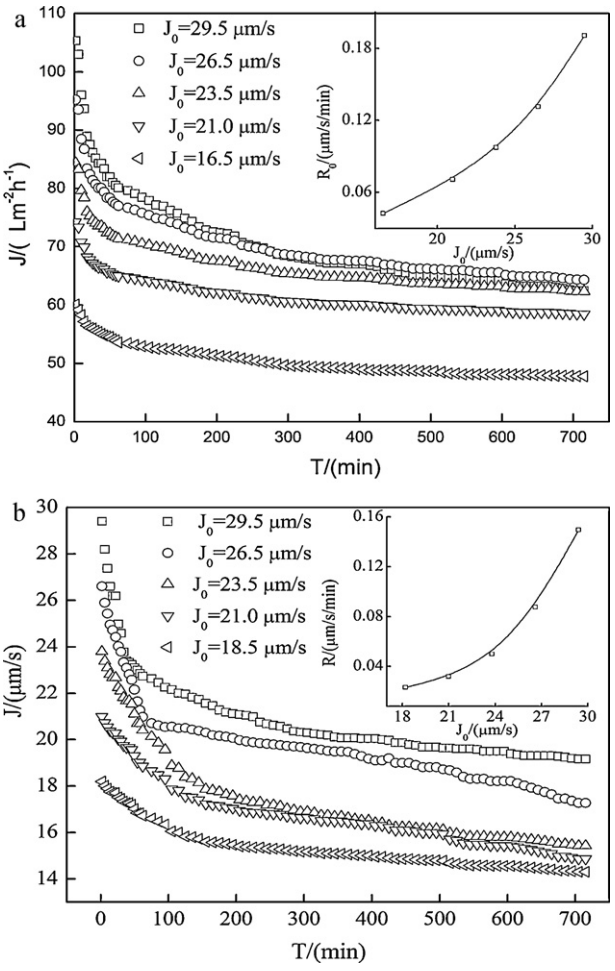

Fig. 8. Effect of initial flux on the membrane CPA2 fouling: (a) MB fouling and (b) RB fouling. The inset shows non-linear regression fit of the Langmuir–Hinshelwood equation. Experimental conditions were identical to those in Fig. 4.

fouling increases with increasing dyes concentration due to the interaction. The recovery after chemical cleaning is determined by the amount of dyes adsorbed onto the membrane surface. The anomaly in the fouling profile with RB is attributed to the micellisation. Dynamic light scattering data in the inset of Fig. 9b suggest that the aggregate size and size distribution are strongly influenced by the RB concentration. At the high concentration, the RB molecules assemble as micelle-like structures that do not decrease flux [5,16]. To further verify the results, the contact angles of RO membranes fouled by various RB concentrations are conducted. The contact angles are 41.21 ± 0.88°, 47.69 ± 1.22°, 51.41 ± 1.14° and 42.25 ± 1.54° corresponding to RB concentration of 2, 3, 4, and 6 μM. When the membranes were fouled by RB, the membrane surfaces became more hydrophobic due to the adsorption of RB molecules on membrane surfaces. With increasing RB concentration, the membrane hydrophobicity increased, implying enhanced adsorption of RB. On the contrary, the contact angles decreased, resulting in the increase of the permeate flux.

3.4.3. Effects of calcium

The influences of calcium ions on the fouling potential of dyes at concentration 2.0 μM were studied at 30 °C. And the resultant flux profiles are shown in Fig. 10. As observed, the permeate flux decline decreased with the increasing calcium ions concentration. It was also found that upon the chemical cleaning, the reversibility of flux loss increased with increasing Ca^{2+} concentration.

The presence of Ca^{2+} competes with the cationic dyes for adsorption sites. Calcium ions possess higher charge density than dye molecules, and are preferred to be adsorbed on the negatively charged membrane surface. Furthermore, the adsorption of Ca^{2+} leads to reduction in electrostatic attraction between dye molecules and the membrane. Therefore, the amount of MB and RB adsorption decreases in the presence of Ca^{2+}. The total amount sorption and the irreversible amount sorption with various Ca^{2+} concentrations were calculated by Eqs. (3) and (5), respectively. The results are shown in Table 2. It is noted that the adsorption amount decreased with the increasing calcium ions concentration just like the permeate flux. However, the fouling tended to increase at Ca^{2+}

Table 2
The amount of adsorption on the membrane surface with respect to Ca^{2+} concentration.

Compound	Ca^{2+} concentration (mM)	Total amount of sorption (μmol/m²)	Irreversible amount sorption (μmol/m²)
MB	0	741.2	341.3
	0.5	705.2	308.2
	1.0	602.5	252.3
	2.0	541.3	211.4
RB	0	578.4	283.3
	1.0	481.2	233.3
	2.0	423.1	195.2

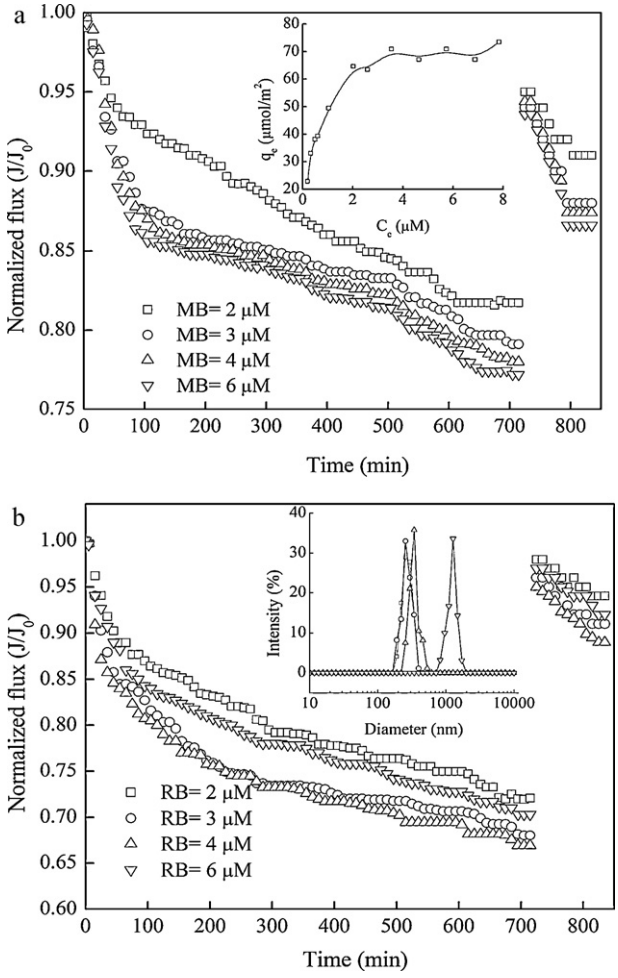

Fig. 9. Effect of dye concentration on dye fouling: (a) MB fouling PROC10 and (b) RB fouling ESPA2. The inset shows (a) Langmuir isotherm of MB adsorbed onto PROC10 at 30 ± 0.5 °C and (b) dynamic light scattering size distributions for RB with different concentrations. Experimental conditions: ionic strength = 10 mM, pH = 7.0 and temperature = 30 ± 0.5 °C. Note that the data points after 715 min are for flux measured with DI water containing salts after the cleaning.

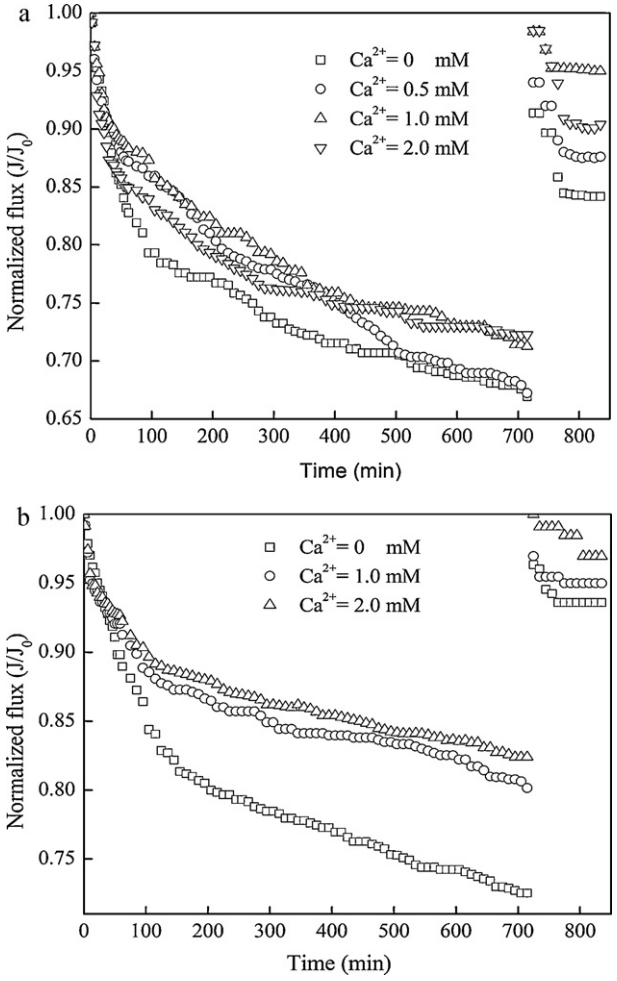

Fig. 10. Effect of calcium concentration on dye fouling of the RO membrane: (a) MB fouling ESPA2 and (b) RB fouling CPA2. Note that the data points after 715 min are for flux measured with DI water containing salts after the cleaning.

concentration of 2.0 mM in the presence of MB. The flux recovery after the membrane was cleaned by EDTA (95.2%) is higher than by SDS (90.5%). Mo et al. have suggested that Ca^{2+} is preferentially adsorbed compared to Na^{+} on the membrane surface [18]. These results suggest that calcium play a dominant role on MB fouling at the high Ca^{2+} concentration.

As depicted in Fig. 10, we also find that the initial fouling rates were almost the same. Hence, it can be inferred that the initial interaction between dyes and the membrane is mainly controlled by dyes concentration, whereas interaction between dyes in the bulk solution and dyes in the fouling layer is mostly governed by calcium ion concentration. With relation to the competition model, the interaction can be related to the synergetic effects of shielding effect and competition effect between Ca^{2+} and cationic dyes molecules.

3.4.4. Effects of magnesium

Fig. 11 is clearly described the influence of the magnesium on the flux decline. In the experiments, the total ionic strength was kept constant at 10 mM and solution pH was kept constant at 7.0. The results clearly demonstrate that permeate flux decline decreased slightly in the presence of magnesium. It was also observed that upon the chemical cleaning, the reversibility of flux loss increased after the addition of magnesium ion. Magnesium ions possess higher charge density than calcium ions [39], and shows greater shielding effect and competition effect than Ca^{2+} and Na^{+}. However the fouling in the presence of magnesium decreased less significantly than that observed in the presence of calcium. To prove the results, the adsorption of dyes on the membrane surface was calculated, and the results are shown in Table 3. The results from Tables 2 and 3 clearly indicate that the adsorption amount of dye molecules in the present of Mg^{2+} is higher than that in the present of Ca^{2+} at the same concentration. Another interesting finding was that initial fouling rates increased at a fixed RB concentration 2 μM. The RB fouling at the initial stage seemed to be opposite to the competition model in the presence of Mg^{2+}. This anomaly in the fouling profile is probably attributed to other interactions apart from the electrostatic interaction, which is most likely the for-

Table 3
The amount of adsorption on CPA2 surface with respect to Mg^{2+} concentration.

Compound	Mg^{2+} concentration (mM)	Total amount of sorption (μmol/m²)	Irreversible amount sorption (μmol/m²)
MB	0	700.4	390.7
	1.0	632.3	289.3
	2.0	571.6	232.4
RB	0	578.4	283.3
	1.0	510.3	245.6
	2.0	475.6	223.2

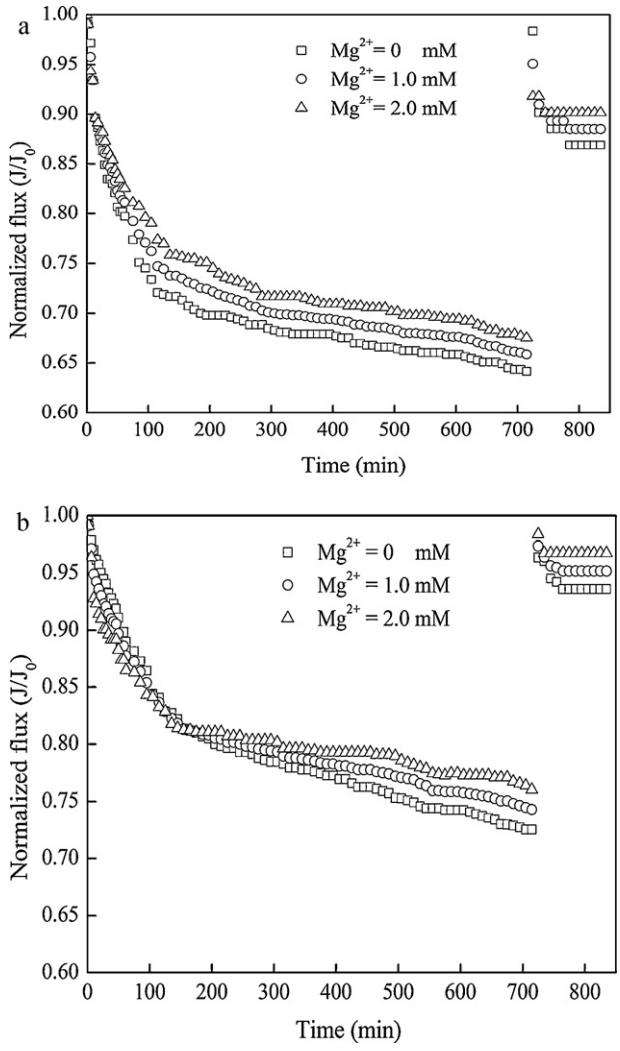

Fig. 11. Effect of magnesium concentration on dye fouling of the RO membrane CPA2: (a) MB and (b) RB. Note that the data points after 715 min are for flux measured with DI water containing salts after the cleaning.

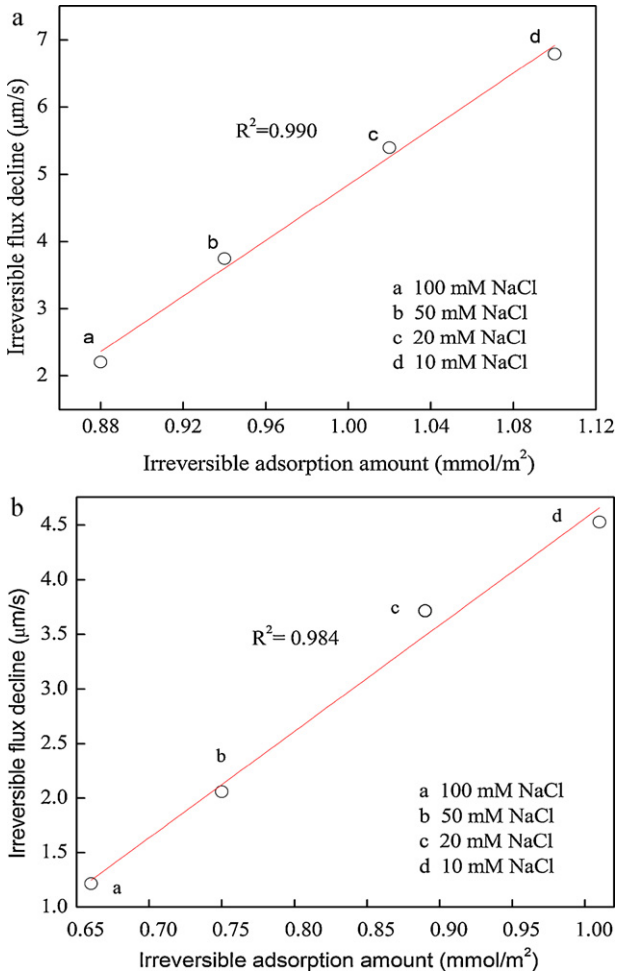

Fig. 12. Correlation between the irreversible flux decline and the irreversible adsorption amount with respect to NaCl concentration during CPA2 fouling: (a) MB and (b) RB.

mation of ionic bridge between adjacent carboxyl groups in RB and aromatic polyamide chains [40]. However, the dissociation of carboxyl groups in RB structure is so weak at pH 7.0 that the competition for adsorption site has replaced the binding effect at long fouling times.

3.5. Correlation between fouling and adsorption

The results presented earlier in this study suggest that organic fouling behavior is controlled by the adsorption of contaminants. The flux decline can be divided by reversible and irreversible flux decline. Reversible and irreversible flux decline were not distinguished in many previous studies. As a result, knowledge of irreversible flux decline occurring in membrane based purification of secondary wastewater effluents for recycling is scarce. Based on the effectiveness of chemical cleaning selected in this study, we correlate the irreversible flux decline to the corresponding irreversible adsorption amount. The flux decline and adsorption amount were studied after 4 cycles of fouling-cleaning procedures. And the corresponding correlations between the irreversible flux decline and the adsorption amount are shown in Fig. 12.

When the ionic strength was increased from 10 to 100 mM, irreversible extent of fouling was observed to decrease in experiments. The competing effect enhanced by the increases in cation (Na^+) with ionic strength reduced the adsorption site on the membrane surface. A striking correlation between the irreversible flux decline and the irreversible adsorption amount is displayed for the runs with NaCl. The strong correlation between adsorption amount and flux decline depicted in Fig. 12 clarifies that the decline of membrane surface area by adsorption serves as the dominant fouling potential.

4. Conclusion

Well-controlled fouling-cleaning experiments were conducted to investigate the correlation between the membrane fouling behaviors and the adsorption of dyes. The following conclusions were extracted from the study.

1. Flux decline in aqueous solutions containing organic compounds is mainly controlled by the adsorption, enhanced by cake formed on the membrane surface.
2. The L–H kinetics rate model was applied to the organic fouling, with kinetic value $k = 0.0556\ \mu m\ s^{-1}\ min^{-1}$ and $k = 0.0181\ \mu m\ s^{-1}\ min^{-1}$ for MB and RB fouling RO membrane CPA2.
3. The extent of flux decline decreases with higher divalent cation concentration due to the competition between divalent cation and dye molecules for the adsorption site on the membrane surface.

4. A striking correlation between the irreversible flux decline and the irreversible adsorption amount was obtained. This direct relationship confirms that irreversible adsorption plays a crucial role in determining the extent of irreversible organic fouling.

Acknowledgements

This work was supported by the Plan of the National Sci-Tech Major Special Item for Water Pollution Control and Management (2009ZX07528-003-05) and the Fundamental Research Funds for the Central Universities (FRFCU), China (A ward No. 20102030201000043). We would like to thank Nitto Denko for providing the membrane samples used in this study.

References

[1] M. Zhou, P.R. Nemade, X. Lu, X. Zeng, E.S. Hatakeyama, R.D. Noble, D.L. Gin, New type of membrane material for water desalination based on a cross-linked bicontinuous cubic lyotropic liquid crystal assembly, J. Am. Chem. Soc. 129 (2007) 9574–9575.
[2] S. Lee, M. Elimelech, Relating organic fouling of reverse osmosis membranes to intermolecular adhesion forces, Environ. Sci. Technol. 40 (2006) 980–987.
[3] W.S. Ang, M. Elimelech, Fatty acid fouling of reverse osmosis membranes: implications for wastewater reclamation, Water Res. 42 (2008) 4393–4403.
[4] G. Chen, X. Chai, P.L. Yue, Y. Mi, Treatment of textile desizing wastewater by pilot scale nanofiltration membrane separation, J. Membr. Sci. 127 (1997) 93–99.
[5] T. Srisukphun, C. Chiemchaisri, T. Urase, K. Yamamoto, Experimentation and modeling of foulant interaction and reverse osmosis membrane fouling during textile wastewater reclamation, Sep. Purif. Technol. 68 (2009) 37–49.
[6] L. Braeken, B. Van der Bruggen, C. Vandecasteele, Flux decline in nanofiltration due to adsorption of dissolved organic compounds: model prediction of time dependency, J. Phys. Chem. B 110 (2006) 2957–2962.
[7] T. Mohammadi, M. Kazemimoghadam, M. Saadabadi, Modeling of membrane fouling and flux decline in reverse osmosis during separation of oil in water emulsions, Desalination 157 (2003) 369–375.
[8] A. Asatekin, S. Kang, M. Elimelech, A.M. Mayes, Anti-fouling ultrafiltration membranes containing polyacrylonitrile-graft-poly (ethylene oxide) comb copolymer additives, J. Membr. Sci. 298 (2007) 136–146.
[9] L. Braeken, K. Boussu, B. Van der Bruggen, C. Vandercastelle, Modeling of the adsorption of organic compounds on polymeric nanofiltration membranes in solutions containing two compounds, Chem. Phys. Chem. 6 (2005) 1606–1612.
[10] Q. Li, Z. Xu, I. Pinnau, Fouling of reverse osmosis membranes by biopolymers in wastewater secondary effluent: role of membrane surface properties and initial permeate flux, J. Membr. Sci. 290 (2007) 173–181.
[11] B. Van der Bruggen, L. Braeken, C. Vandecasteele, Flux decline in nanofiltration due to adsorption of organic compounds, Sep. Purif. Technol. 29 (2002) 23–31.
[12] P. van den Brink, A. Zwijnenburg, G. Smith, H. Temmink, M. van Loosdrecht, Effect of free calcium concentration and ionic strength on alginate fouling in cross-flow membrane filtration, J. Membr. Sci. 345 (2009) 207–216.
[13] W.Y. Ahn, A.G. Kalinichev, M.M. Clark, Effects of background cations on the fouling of polyethersulfone membrane by natural organic matter: experimental and molecular modeling study, J. Membr. Sci. 309 (2008) 128–140.
[14] Q. Li, M. Elimelech, Organic fouling and chemical cleaning of nanofiltration membrane: measurements and mechanisms, Environ. Sci. Technol. 38 (2004) 4683–4693.
[15] X. Jin, X. Huang, E.M.V. Hoek, Role of specific ion interactions in seawater RO membrane fouling by alginic acid, Environ. Sci. Technol. 43 (2009) 3580–3587.
[16] H. Li, Y. Lin, P. Yu, Y. Luo, L. Hou, FTIR study of fatty acid fouling of reverse osmosis membranes: effects of ph, ionic strength, calcium, magnesium and temperature, Sep. Purif. Technol. 77 (2011) 171–178.
[17] X. Zhu, M. Elimelech, Colloidal fouling of reverse osmosis membrane: measurements and fouling mechanisms, Environ. Sci. Technol. 31 (1997) 3654–3662.
[18] H. Mo, K.G. Tay, H.Y. Ng, Fouling of reverse osmosis membrane by protein (BSA): effects of pH, calcium, magnesium, ionic strength and temperature, J. Membr. Sci. 315 (2008) 28–35.
[19] S. Lee, W.S. Ang, M. Elimelech, Fouling of reverse osmosis membranes by hydrophilic organic matter: implications for water reuse, Desalination 187 (2006) 313–321.
[20] W. Lee, C.H. Ahn, S. Hong, S. Kim, S. Lee, Y. Baek, J. Yoon, Evaluation of surface properties of reverse osmosis membranes on the initial biofouling stages under no filtration condition, J. Membr. Sci. 351 (2010) 112–122.
[21] E.M.V. Hoek, S. Hong, M. Elimelech, Influence of membrane surface properties on initial rate of colloidal fouling of reverse osmosis and nanofiltration membranes, J. Membr. Sci. 188 (2001) 115–128.
[22] F. Fairbrother, H. Mastin, Studies in electro-endosmosis, J. Chem. Soc. 125 (1924) 2319–2330.
[23] W.S. Ang, S. Lee, M. Elimelech, Chemical and physical aspects of cleaning of organic-fouled reverse osmosis membranes, J. Membr. Sci. 272 (2006) 198–210.
[24] S. Eftekhari, A. Habibi-Yangjeh, S. Sohrabnezhad, Application of A1MCM-41 for competitive adsorption of methylene blue and rhodamine B: thermodynamic and kinetic studies, J. Hazard. Mater. 178 (2010) 349–355.
[25] S. Merouani, O. Hamdaoui, F. Saoudi, M. Chiha, Sonochemical degradation of Rhodamine B in a aqueous phase: effects of additives, Chem. Eng. J. 158 (2010) 550–557.
[26] E. Steinle-Darling, E. Litwilier, M. Reinhard, Effects of sorption on the rejection of trace organic contaminants during nanofiltration, Environ. Sci. Technol. 44 (2010) 2592–2598.
[27] W. Lee, C.H. Ahn, S. Hong, S. Kim, S. Lee, Y. Baek, J. Yoon, Evaluation of surface properties of reverse osmosis membrane on the initial biofouling stages under no filtration condition, J. Membr. Sci. 351 (2010) 112–122.
[28] R.M. Silverstein, F.X. Webster, D. Kiemle (Eds.), Spectrometric Identification of Organic Compounds, seven ed., John Wiley & Sons Inc., Hoboken, 2005.
[29] M.R. Hoffmann, S.T. Martin, W. Choi, D.W. Bahnemann, Environmental applications of semiconductor photocatalysis, Chem. Rev. 95 (1995) 69–96.
[30] C.S. Turchi, D.F. Ollis, Photocatalytic degradation of organic water contaminants: mechanisms involving hydroxyl radical attack, J. Catal. 122 (1990) 178–192.
[31] A. David, M.A. Vannice, Control of catalytic debenzylation and dehalogenation reactions during liquid-phase reduction by H_2, J. Catal. 237 (2006) 349–358.
[32] K. Listirini, W. Chun, D.D. Sun, J.O. Leckie, Fouling mechanism and resistance analyses of systems containing sodium alginate, calcium, alum and their combination in dead-end fouling of nanofiltration membranes, J. Membr. Sci. 344 (2009) 244–251.
[33] S.S. Madaeni, S. Samieirad, Chemical cleaning of reverse osmosis membrane fouled by wastewater, Desalination 257 (2010) 80–86.
[34] M. Bartlett, M.R. Bird, J.A. Howell, An experimental study for the development of a qualitative membrane cleaning model, J. Membr. Sci. 105 (1995) 147–157.
[35] S. Lee, M. Elimelech, Salt cleaning of organic-fouled reverse osmosis membranes, Water Res. 41 (2007) 1134–1142.
[36] A. Seidel, M. Elimelech, Coupling between chemical and physical interactions in natural organic matter (NOM) fouling of nanofiltration membranes: implications for fouling control, J. Membr. Sci. 203 (2002) 245–255.
[37] S. Wang, Z.H. Zhu, Characterisation, environmental application of an Australian natural zeolite for basic dye removal from aqueous solution, J. Hazard. Mater. 136 (2006) 946–952.
[38] S.K. Alpat, O. Ozbayrak, S. Alpat, H. Akcay, The adsorption kinetics and removal of cationic dye, Toluidine Blue O, from aqueous solution with Turkish zeolite, J. Hazard. Mater. 151 (2008) 213–220.
[39] M.H. Tran-Ha, V. Santos, D.E. Wiley, The effect of multivalent cations on membrane-protein interactions during cleaning with CTAB, J. Membr. Sci. 251 (2005) 179–188.
[40] W.S. Ang, M. Elimelech, Protein (BSA) fouling of reverse osmosis membranes: implications for wastewater reclamation, J. Membr. Sci. 296 (2007) 83–92.